EFDA–JET–PR(08)60

V. Parail, P. Belo, P. Boerner, X. Bonnin, G. Corrigan, D. Coster, J. Ferreira, A. Foster, L. Garzotti, G.M.D. Hogeweij, W. Houlberg, F. Imbeaux, J. Johner, F. Kochl, V. Kotov, L. Lauro-Taroni, X. Litaudon, J. Lonnroth, G. Pereverzev, Y. Peysson, G. Saibene, R. Sartori, M. Schneider, G. Sips, P. Strand, G. Tardini, M. Valovic, S. Wiesen, M. Wischmeier, R. Zagorski, EU ITM Task Force and JET EFDA contributors

Integrated Modelling of ITER Reference Scenarios

Integrated Modelling of ITER Reference Scenarios

V. Parail[1], P. Belo[2], P. Boerner[3], X. Bonnin[4], G. Corrigan[1], D. Coster[12], J. Ferreira[2], A. Foster[5], L. Garzotti[1], G.M.D. Hogeweij[6], W. Houlberg[7], F. Imbeaux[8], J. Johner[8], F. Kochl[9], V. Kotov[3], L. Lauro-Taroni[10], X. Litaudon[8], J. Lonnroth[11], G. Pereverzev[12], Y. Peysson[8], G. Saibene[13], R. Sartori[13], M. Schneider[8], G. Sips[12], P. Strand[14], G. Tardini[12], M. Valovic[1], S. Wiesen[3], M. Wischmeier[12], R. Zagorski[15], EU ITM Task Force and JET EFDA contributors*

JET-EFDA, Culham Science Centre, OX14 3DB, Abingdon, UK

[1]EURATOM/UKAEA Fusion Association, Culham Science Centre, Abingdon OX14 3DB, United Kingdom
[2]Association Euratom-IST, Lisboa, Portugal
[3]Institut für Energie Forschung-Plasma Physik,Forschungszentrum Juelich GmbH, Germany
[4]LIMHP, CNRS-UPR, Université Paris 13, Villetaneuse, France
[5]Department of Physics, Univ. of Strathclyde, Glasgow, UK
[6]FOM-Institute for Plasma Physics Rijnhuizen, NL-3430 BE Nieuwegein, The Netherlands
[7]ITER Organisation, 13108 St Paul lez Durance, France
[8]Association Euratom-CEA, Cadarache 13108 Saint Paul LEZ DURANCE, FRANCE
[9]Association EURATOM-ÖAW/ATI, Vienna, Austria
[10]Associazione EURATOM-ENEA sulla Fusione, Consorzio RFX Padova, Italy
[11]Association EURATOM-TEKES, Helsinki University of Technology, P.O. Box 2200, FIN-02015 HUT, Finland
[12]Max-Planck-Institut für Plasmaphysik, EURATOM-Assoziation, D-85748, Garching, Germany
[13]FUSION FOR ENERGY Joint Undertaking, 08019 Barcelona (Spain)
[14]Chalmers University, Gothenburg, Sweden
[15]EFDA Close Support Unit, Garching, Germany
** See annex of F. Romanelli et al, "Overview of JET Results",*
(Proc. 22 [nd] IAEA Fusion Energy Conference, Geneva, Switzerland (2008)).

Preprint of Paper to be submitted for publication in
Nuclear Fusion

ABSTRACT.
The ITER Scenario Modelling Working Group (ISM WG) is organised within the European Task Force on Integrated Tokamak Modelling (ITM-TF). The main responsibility of the WG is to advance a pan-European approach to integrated predictive modelling of ITER plasmas with the emphasis on urgent issues, identified during the ITER Design Review. Three major topics are discussed, which are considered as urgent and where the WG has the best possible expertise. These are modelling of current profile control, modelling of density control and impurity control in ITER (the two last topics involve modelling of both core and SOL plasma). Different methods of heating and current drive are tested as controllers for the current profile tailoring during the current ramp up in ITER. These include Ohmic, NBI, ECRH and LHCD methods. Simulation results elucidate the available operational margins and rank different methods according to their ability to meet different requirements. A range of "ITER-relevant" plasmas from existing tokamaks were modelled. Simulations confirmed that the theory-based transport model, GLF23, reproduces the density profile reasonably well and can be used to assess ITER profiles with both pellet injection and gas puffing. In addition, simulations of the SOL plasma were launched using both H-mode and L-mode models for perpendicular transport within the edge barrier and in the SOL. Finally, an integrated approach was also used for the predictive modelling of impurity accumulation in ITER. This includes helium ash, extrinsic impurities (like argon) and impurities coming from the wall (including tungsten). The relative importance of anomalous and neo-classical pinch contributions towards impurity penetration through the edge transport barrier and further accumulation in the core was assessed.

1. MODELLING OF CURRENT PROFILE CONTROL IN ITER

Two aspects of current profile control make modelling of current ramp up/down in ITER an urgent task. First is a concern about the present design of ITER PF system and its ability to ensure reliable operation of all ITER reference scenarios. Secondly, it is important to ensure that H&CD and PF systems have enough flexibility to generate any current profile and to keep it as long as it might be needed by one, or the other, ITER reference scenarios.

Predictive modelling of current profile evolution in ITER was done using two core transport codes Cronos [1] and Jetto [2]. Both codes have fixed boundary equilibrium solvers so they require information about the magnetic boundary evolution from other codes. After that the task is reduced to a numerical solution of transport equations for toroidal current and electron and ion temperature in the plasma core with given density and Z_{eff} profiles. The following heating/current drive schemes were tested: Ohmic, Electron Cyclotron Resonance Heating (ECRH), Neutral Beam Injection (NBI), Lower Hybrid Current Drive (LHCD), with power and current deposition profiles calculated by internal solvers. Since both electrical conductivity (which is assumed to be neo-classical) and power and current deposition profiles for Ohmic, ECRH and LHCD depend mainly on electron temperature, the choice of the transport model for electron transport is essential. Three different transport models were used in predictive modelling of ITER scenarios, presented in this paper. First is a well-known

theory-based transport model GLF23 [3]. Since model is quite stiff, the temperature prediction in the core has a strong dependence on the edge plasma parameters, which are not well known for L-mode plasma. We therefore use it only to simulate plasma performance during flattop burn. For the current ramp modelling, another heat transport model, a priori much less sensitive to the boundary condition, has been used. The heat diffusion coefficients are written as:

$$\chi_e = \chi_i = f \cdot (1 + 6\rho^2 + 80\rho^{20}) \quad (1)$$

where f is dynamically adjusted during the run to keep energy confinement time as a given fraction of ITER-98(y2) confinement scaling [4] (usually 0.4<H98y<0.5) and ρ is a square root of normalised toroidal flux. The third model is a well-known (and tested) empirical JET Bohm/gyroBohm model [5]. Needless to say, all three models have to be tested on relevant experimental data before they are used to predict ITER plasma.

1.1 SIMULATION OF CURRENT RAMP UP/DOWN IN JET

A few recent ITER-relevant JET plasmas with either Ohmic or LH-assisted current ramp up/down were selected to test transport models. Figures 1 and 2 show the result of this test for 2 JET Ohmic pulses with different I_p ramp rate (see [6,7]) using empirical transport models. One can conclude that both transport codes reproduce both the current penetration (l_i time trace and q-profiles) and the heat transport (W_{the} time trace and T_e profiles) quite well and agree with each other when both codes use either Bohm/gyroBohm model or empirical formula (1) and keep H98y=0.4 for L-mode. A similar conclusion can be drawn when Bohm/gyroBohm model was applied to JET current ramp down plasma, if the model is applied after the plasma returns to L-mode. It is worth noting that all above mentioned JET plasmas were considered as prototypes of ITER baseline Scenario-2 ELMy H-mode or hybrid Scenario-3 and therefore they do not require development of a non-monotonic q-profile, which is needed for steady-state plasma with internal transport barrier (ITER Scenario-4). JET has also carried out a dedicated experiment on current ramp-up with assistance from LHCD system with P_{LH}=2MW (also about 1.5MW of NBI power was added for T_i and q-profile measurements). These well-diagnosed discharges were also used to benchmark the LH ray tracing and beam tracing codes available in CRONOS and JETTO, with the stand-alone code LUKE [8]. As expected, simulations of current diffusion show strong sensitivity of current profile evolution with respect to electron temperature profile, LH wave spectrum and assumptions about radial broadening of the predicted LH current. Reasonable agreement between the CRONOS and JETTO codes in terms of generation of LH current was obtained (see Figure 3), although in some cases noticeable difference between both codes and LUKE was observed in the position and shape of LH power and current density. Also, there is a conspicuous difference in time evolution of simulated and measured l_i and loop voltage V_{loop}, which might be related to the difference in LH current profile. Note that some important macroscopic discharge characteristics (like internal inductance l_i and V_{loop}) depend not only on LH current drive but also on plasma heating due to LH waves (compare with ECH heating in ITER, Figure 5). More work is

needed to resolve the precise role of LH current drive and LH heating in shaping the q-profile in JET and ITER plasma.

1.2 MODELLING OF CURRENT RAMP UP IN ITER

Two important questions to be addressed are: *(i)* how much heating power and current drive is required in ITER to reach the target q-profile for various scenarios; *(ii)* how can one minimise the flux consumption. A number of scans were done, including a density scan, a scan in magnetic configuration and scan in additional (ECRH) heating to address these issues. Very good agreement was obtained between CRONOS and JETTO in local profiles (T_e, q, j_z) and time evolving global characteristics (l_i, V_{loop}, flux consumption and W_{th}). Only the current profile and ion and electron temperature profiles were predicted using the scaling based transport model (1) with ion densities and Z_{eff} assumed. It was also assumed that plasma stays in L-mode for the whole ramp up phase. Note that this model has been only validated against Ohmic current ramp up. Work is in progress to test it in cases with additional heating such as ECRH or LHCD. Note also that both fixed and evolved boundaries from [9] were used.

Figures 4 and 5 present the results of two scans: (a) a density scan from $n=0.15n_G$ to $n=0.4n_G$ ($n_G=I_p/\pi a^2$); (b) a scan of off-axis ECH power from 0 to 20 MW; the power is assumed to be localized at mid-radius with a narrow Gaussian deposition profile; no current drive is assumed. It is seen that the q profile at the start of the flat-top is flat with Ohmic heating, and is moderately hollow with 10 MW of off-axis ECH. The latter q profile comes close to the target profile for hybrid scenarios. Moreover, off-axis heating is crucial to keep l_i below $l_i<1$ during the current ramp phase. Work is in progress to assess the effectiveness of LHCD in shaping the q profile during current ramp up in ITER.

2. PREDICTIVE MODELLING OF ITER PLASMA FUELLING BY PELLETS

Fully predictive simulations of ITER Scenario 2 in the H-mode phase have been carried out with JETTO and ASTRA [10] to investigate the effect of pellet injection from the high field side (HFS) on plasma performance for different assumptions regarding the outward horizontal drift of the ablated pellet material. In the plasma core, the GLF-23 model together with neo-classical transport has been used for predictive modelling of T_e, T_i, n_D and n_T (Z_{eff} profile was fixed). Transport within the ETB was emulated by an empirical continuous ELM model. Within the ETB, a constant normalised pressure gradient $\alpha_{crit.} = 2.0$ to 2.5 ($\alpha=-(2m_0Rq^2/B^2)dp/dr$, the range of applied α_{crit} was confirmed by MHD stability analysis) is maintained using an empirical ELM model with the additional transport due to ELM events spread continuously over time. The transport coefficients within the ETB are calculated as follows:

$$\chi_{e,i} = \chi_{e,i\ neocl} + C_{1,2} \cdot \max\left(0,\ \frac{\alpha}{\alpha_{crit}} - 1\right)^{\beta}\ [\mathrm{m^2/s}],$$
$$D = D_{neocl} + C_3 \cdot \max\left(0,\ \frac{\alpha}{\alpha_{crit}} - 1\right)^{\beta}\ [\mathrm{m^2/s}], \qquad (2)$$

with $\chi_{e,i}$ the electron or ion heat diffusivity, $\chi_{e,i\ neocl.}$ being electron or ion neo-classical diffusivity, D and $D_{neocl.}$ the respective values for particle diffusivity and neo-classical diffusivity, $C_{1\text{-}3}$ constant multipliers ($C_1 = C_2 = C_3 = 100$ were used in simulations), α the maximum normalised pressure gradient within the ETB, and β an exponential parameter ($\beta = 2.5$ was used in simulations). The pellet source profiles were either provided by the JETTO-internal NGPS pellet model [11] or an externally coupled first-principles pellet code developed at Cadarache [12]. It could be shown that the pellet particle penetration and the fuelling efficiency strongly depend on the expected pellet drift (it is assumed that all pellets were injected into the plasma from High Field Side (HFS)). Simulations with transport code ASTRA were done using the pellet particle source from JETTO.

These simulations address the following issues: *(i)* what will be the main ion density profile in ITER with a shallow localised particle source; *(ii)* how much plasma performance, in general (and main ion confinement in particular), depends on how deep pellets drift into plasma core; *(iii)* how much particle throughput depends on pellet penetration. It is important to stress here that since pellet ablation is very shallow, the radial distribution of ablated material and its further drift depend sensitively on plasma parameters near the separatrix (fixed in these simulations). Therefore self-consistent modelling of the SOL plasma, as well as the core plasma, is mandatory for future research. Simulation results for 10s runs with the model [12], applying 0%, 50% and 100% of the calculated pellet drift displacement, are shown in Figs.6-8. Pellet composition is assumed to be 50%D and 50%T with the pellet size 5mm (cubic shape) and speed 300m/s. The average density stabilises in all cases at a constant level of $<n_e>=10^{20}\ m^{-3}\ \pm 5\%$ with the axial density reaching $n_e(0)=1.35\times10^{20}\ m^{-3}\ \pm 4\%$ (see Figure 6, note that density feedback control of pedestal density was used in these simulations). Also the average temperature remains roughly constant with time after an equilibration phase of about 2-3 seconds, although the electron temperature and energy content are reduced by 15% in the case of 100% drift mainly because of core cooling by deeply penetrating pellets. The pellet injection frequency stabilises at 5Hz for 0%, 2Hz for 50% and 1.5Hz for 100% pellet drift. The energy confinement time is constant at a level of $\tau_E = 1.65$s, the average particle confinement time τ_p increases from 4s for 0%, to 6s for 50% and to 8s for 100% pellet drift at t = 410s. In all cases the density profile is peaked with the characteristic peaking factor $n_e(0)/<n_e>=1.4$, which is expected from GLF23 model (Figure 7). Deuterium density is slightly more peaked than Tritium density due to D source from NBI. Pellet drift has little effect on the density profile.

Figure 8 shows the deposition profiles of the last injected pellet for all three cases. The maxima are situated at $\rho = 0.98$, 0.91, and 0.84 for 0%, 50% and 100% pellet drift. Due to the high ablation rate already at the very edge of the ITER plasma, the pellet simulations indicate that sufficient pellet particle penetration beyond the ETB and high particle confinement times can only be reached by exploitation of the ∇B-drift for HFS injections at the available injection speeds. Comparing the 0% to the 100% drift case, the particle outflow at the edge is tripled, and the capability of the vacuum pump might reach its limit in the case of 0% drift. According to our results, the time average pumping capability needed in the 0%, 50% and 100% drift case can be estimated to be equal to ~ 55, 30 and 25Pa m^3/s respectively, but in the 0% drift case, the temporary particle outflow

after pellet injection can increase up to $>10^{23}$ particles per second, corresponding to > 200 Pa m^3/s. An additional potential problem with this result is that it only includes particle outflow due to pellets. It is known that external gas puffing is needed on top of core fuelling in order to increase density near the separatrix to a level, which brings the plasma to detachment. Modelling of plasma fuelling by both methods requires self-consistent modelling of core and SOL and we will discuss some preliminary results of such modelling in Section 4. Here we would like to mention another potentially important finding, which comes from exploration of "continuous ELM" model. Our simulations show that even if the contribution to particle diffusion within ETB due to continuous ELMs is equal to the electron and ion thermal conductivity enhancement, its value does not exceed $D=0.1\ m^2/s$ to keep edge pressure gradient below the peeling/ballooning stability limit. Such a low level of heat and particle transport alters conditions, needed for plasma detachment. This will be also discussed in Section 4.

Finally, a combination of the scaling-based transport model (which we use during current ramp up/down phase) and "modified" GLF23 model with continuous ELMs allows full predictive modelling of the ITER Scenario 2 starting from early current ramp up through steady-state burn and finishing by current ramp down. Figure 9 shows some characteristic time traces of such plasma simulations, which demonstrate that with the present knowledge of heat and particle transport it is feasible to get fusion gain Q≈10 in ITER Scenario 2 plasma.

3. STUDY OF IMPURITY ACCUMULATION IN ITER REFERENCE SCENARIOS

Three important questions to address in the area of impurity accumulation in ITER are considered: *(i)* is the present ITER pumping capability adequate to remove He ash from plasma core; *(ii)* is it possible to radiate up to 70% of heat flux from the SOL by recycled impurities like Ar without the risk of plasma core contamination; *(iii)* is it possible to avoid heavy impurity (W) accumulation in the core. All three questions (particularly *(ii)* and *(iii)*) can be adequately answered only if fully self-consistent predictive modelling of the core and SOL is utilized. This is a long term program and here we report the result of our initial investigation, which is effectively limited to predictive modelling of impurity accumulation in plasma core, including the ETB. The same transport model as in Section 2 was used in the JETTO/SANCO to study impurity transport: a combination of GLF23 (for both main ions and impurity) with neo-classical transport in the core and ad hoc transport within the ETB (see (2)) to keep the pressure gradient close to the ballooning stability limit. It is worth noting here that the present implementation of the GLF23 model for impurities (only single impurity is allowed by the model) assumes the impurity is fully ionised. This approach might be adequate for Ne or even Ar in hot ITER plasmas, but it is incorrect in case of W. Therefore our results for W should be considered with caution. It is also worth noting that so-called bundled description of heavy impurities, which sums up impurities within the narrow range of ionisation potential into one effective ionisation stage, was used in these simulations. This method significantly reduces the running time. Figure 10 shows the radial distribution of Ar ions in Scenario 2 ITER plasma during the steady burn phase with two sets of boundary conditions for the main ions. The

solid curve corresponds to high density at the separatrix (and low temperature), when neo-classical pinch velocity is outward directed within ETB. The dashed curve relates to the opposite limiting case, when edge density is low so that the neo-classical pinch velocity is negative within ETB. Note that the same initial Ar content (uniformly distributed over the core and SOL) was used in all runs. One can observe that neo-classical pinch velocity plays a very important role in the redistribution of heavy impurities within the plasma core. The reason is that anomalous transport is almost fully suppressed within the ETB (the level of ad hoc transport to keep pressure gradient below ballooning stability limit is relatively small, particularly for heavy impurities) so the sign of the neo-classical pinch controls the penetration of impurities inside edge barrier. Deeper inside, the impurity content is almost evenly distributed due to strong anomalous diffusion. Since the neo-classical pinch is proportional to impurity charge *Z*, its role is insignificant for light impurities like *N* or *He* ash (see Figure 11). Obviously, the extremely sensitive dependence on the neo-classical impurity pinch of main ions' boundary conditions calls for fully integrated modelling of both core and SOL plasma in ITER. This will be further discussed in the next Section.

4. PREDICTIVE MODELLING OF ITER SCENARIO 2 SOL PLASMA.

It was shown above that both the main ion and impurity behaviour in the plasma core are critically influenced by the conditions in the SOL. It is also true to say that the SOL plasma is equally sensitive with respect to thermal and particle transport in plasma core, particularly within the ETB. Our modelling showed that if ITER manages to operate either without ELMs or with very small frequent ELMs while still keeping edge pressure gradient close to the peeling/ballooning limit, then the effective transport coefficient within ETB ought to fall below χ, $D = 0.1\text{m}^2/\text{s}$. To study how the SOL plasma will react to such a small level of transport, three EDGE2D/EIRENE simulations were launched with the following assumptions about radial transport: Case 1 with†"L-mode" transport $D = 0.3m^2/s, \chi_{e,i} = 1m^2/s$ in the whole simulation domain (starting from top of pedestal up to plasma wall); Case 2 with $D = 0.1m^2/s, \chi_{e,i} = 0.3m^2/s$ in the core and within 5mm outside separatrix. Transport returns to "L-mode" level further out; Case 3 with $D = 0.07m^2/s, \chi_{e,i} = 0.1m^2/s$ in the core and within 5mm outside separatrix. Transport returns to "L-mode" level further out. In all cases ion density at the separatrix is kept at $n_{sep} \approx 4.3\times10^{19}\ m^{-3}$ and total heat flux crossing separatrix P_{sep} = 80MW (50MW go to ions and 30MW to electrons). The main results are shown in Table 1 and Figures 12 and 13, and allow us to draw the following conclusions:

The "L-mode" level of transport allows the plasma to spread heat flux over a wide region in the SOL and plasma reaches full detachment on at least the inner target. This level of transport does not allow the pressure gradient to reach a level close to the ballooning stability limit. This translates into much reduced core plasma performance. A lower level of transport within ETB and in the near SOL recovers good performance, but at the expense of a reduced level of plasma detachment (see Table and Figure 12, 13).

It is worth noting that the present maximum heat load on target plate is 10MW/m^2 [13] and this limit is exceeded in Case 3.Although these simulations were done for a pure plasma without

impurities, preliminary analysis shows that predicted temperature and density profiles near the separatrix and within ETB should not allow impurity accumulation in plasma core, particularly if the ion temperature near the separatrix is kept below $T_{i,sep} < 300eV$. Much more modelling is required to draw any firm conclusion about possible ways to reach good core plasma parameters with a tolerable power load on the target plate in ITER reference scenarios.

SUMMARY AND CONCLUSIONS.

Results of recent integrated predictive modelling of reference ITER scenarios using both core and SOL transport codes are presented with the emphasis given to urgent issues, which could influence ITER design decisions. Analysis confirms an ability of the presently designed ITER PF and H&CD systems to generate a wide range of target q-profiles needed for inductive, hybrid and steady-state operation. Also analysis of the present ITER fuelling capability to refuel plasma core by DT pellets was done using the latest theory-based transport model and recent advances in the modelling of the outward drift of ablated material. Results obtained so far indicate that further detailed modelling of ITER pumping capability is required to assess its ability to cope with plasma fuelling by pellet injection. Finally, an initial study of the SOL plasma with an assumption that both heat and particle transport in the near SOL follows H-mode transport is presented, which shows significant deviation of the SOL plasma parameters from previously obtained results, where the L-mode model for perpendicular transport was used.

ACKNOWLEDGMENTS

This work was partly funded by the United Kingdom Engineering and Physical Sciences Research Council and by the European Communities under the contract of Association between EURATOM and UKAEA. The views and opinions expressed herein do not necessarily reflect those of the European Commission. This work was carried out within the framework of the European Fusion Development Agreement.

REFERENCES

[1]. V. Basiuk et al., Nuclear Fusion **43** (2003) 822
[2]. G. Cennacchi and A. Taroni, JET-IR(88) 03
[3]. R.E. Waltz Phys. Plasmas **4** (1997) 2482
[4]. ITER Physics Expert Groups on Confinement and Transport and Confinement Modelling and Database, ITER Physics Basis Editors and ITER EDA 1999, *Nucl, Fusion* **39** 2175
[5]. A. Taroni et al., PPCF 36 (1994) 1629
[6]. A.C.C. Sips et al., 35th Conf on Plasma Physics, Hersonissos, Crete, Greece, 2008
[7]. G.M.D. Hogeweij et al., ibid
[8]. J. Decker and Y. Peysson, Technical report EUR-CEA-FC-1736, December 2004
[9]. C. Kessel et al., this conference IT/2-3

[10]. G.V. Pereverzev et al., ASTRA: Automated System for Transport Analysis in Tokamak, Max-Planck Institutes Report, IPP 5/98

[11]. L. Garzotti et al, Nuclear Fusion **17** (1997) 1167

[12]. B. Pégourié et al. Nuclear Fusion **47** (2007) 44-56

[13]. A.S. Kukushkin et al., Nuclear Fusion **43** (2003) 716

	n_{sep} 10^{19}	$T_{i,sep}$ eV	$T_{e,sep}$ eV	n_{top} 10^{19}	$T_{i,top}$ keV	$T_{e,top}$ keV	$n_{target-out}10^{21}$	$T_{i,out}$ eV	$T_{e,out}$ eV	P_{out} MW/m^2	$n_{target-in}10^{21}$	$T_{i,in}$ eV	$T_{e,in}$ eV	P_{in} MW/m^2
1	4.2	260	170	5.3	0.8	0.6	2.4	4.9	5.6	4.2	3	3.1	3.1	3
2	4.4	325	205	7	1.7	1.2	2.3	4.9	5.6	7.5	4	3.1	3.1	4.6
3	4.0	440	235	8	3	2.2	2.3	8.2	17	25	4	6.2	6.8	16

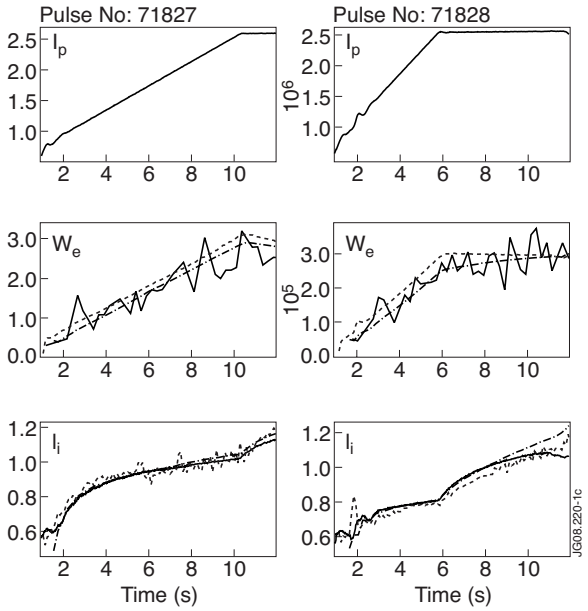

Figure 1: Time evolution of current (top), electron energy content (middle) and internal inductance (bottom): solid-exp, dash-CRONOS, chain-JETTO.

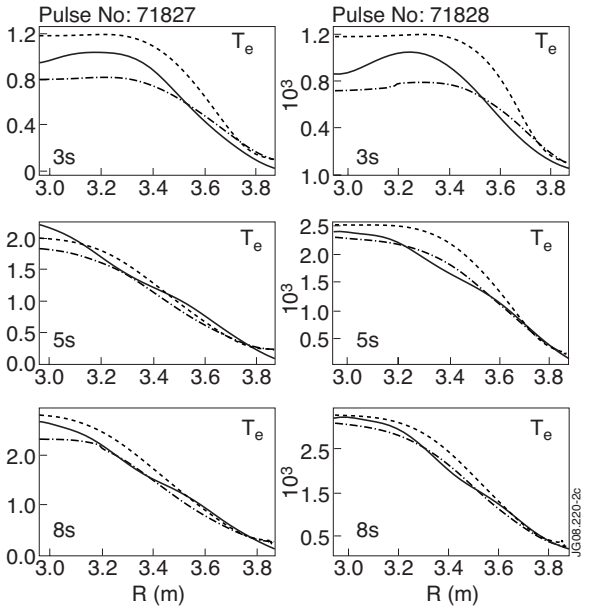

Figure 2: Electron temperature profiles at t = 2sec (top),t = 5sec (middle) and t = 8sec (bottom): solid-exp, dash-CRONOS, chain-JETTO.

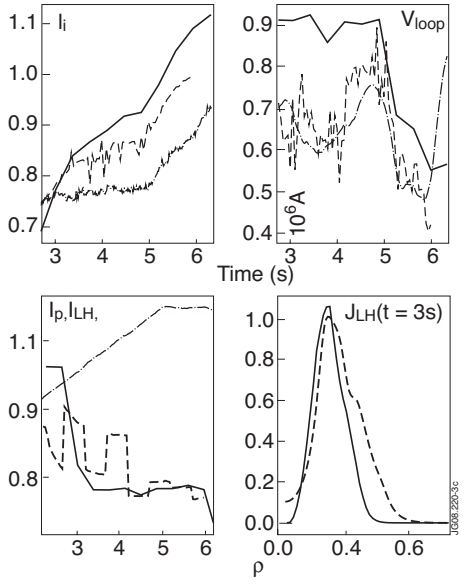

Figure 3: JET Pulse No: 72823, time traces of (clockwise): internal inductance, loop voltage, current and LH current profile (solid-experiment, dash-CRONOS and chain- JETTO.

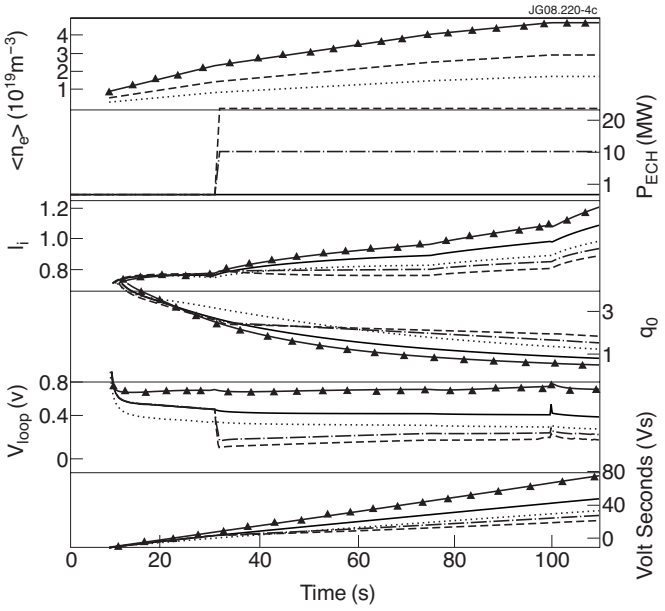

Figure 4: Effect of varying input power and density during ITER current ramp up. The reference simulation (solid lines) has $<n_e>$=0.25 n_G, without additional input power. Shown are simulations with 10MW and 20MW of ECRH off-axis heating starting at 30s, at the same density (chain and dashed lines respectively). Also shown are simulations with $<n_e>$ = 0.15 n_G and 0.4 n_G without additional input power (solid triangles and dots respectively). The panels from top to bottom give $<n_e>$, P_{ECRH}, l_i, q(0), V_{loop} and the flux consumption.

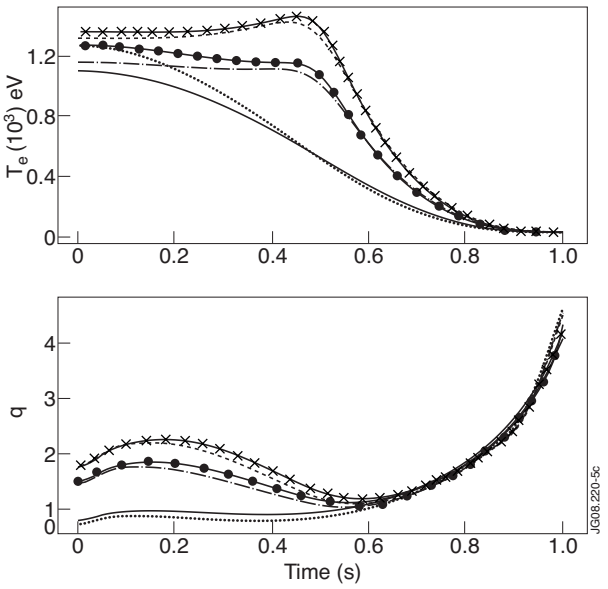

Figure 5: Final profiles of T_e (top) and q (bottom) after 100 s for the ECRH power scan of Figure 4. 0MW ECRH: Solid-CRONOS, dotted-JETTO; 10MW ECRH: chain-CRONOS, solid circles-JETTO; 20MW ECRH: line with crosses– JETTO, dashed line- CRONOS.

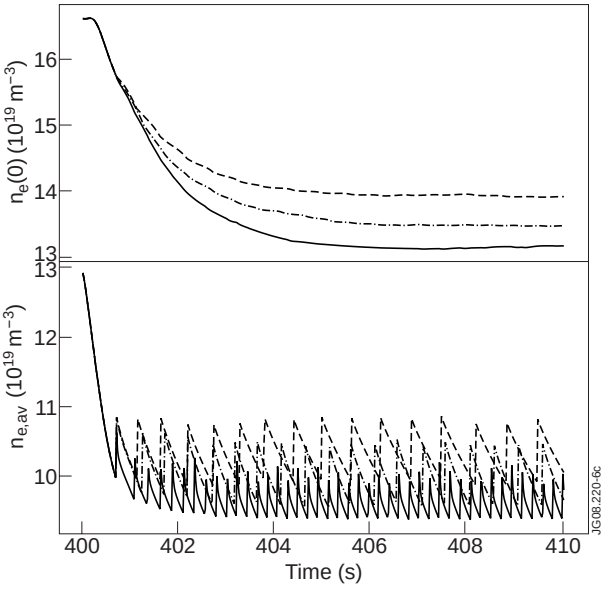

Figure 6: Axial electron density (top) and average electron density (bottom); solid- 0% drift, chain - 50% drift, dash - 100% drift.

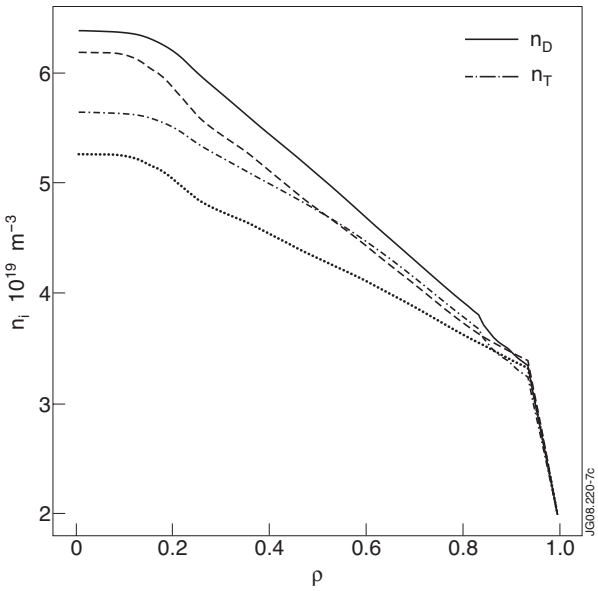

Figure 7: Deuterium density- solid: 100% drift, dashed: 0% drift, Tritium density-chain: 100% drift, dotted: 0% drift.

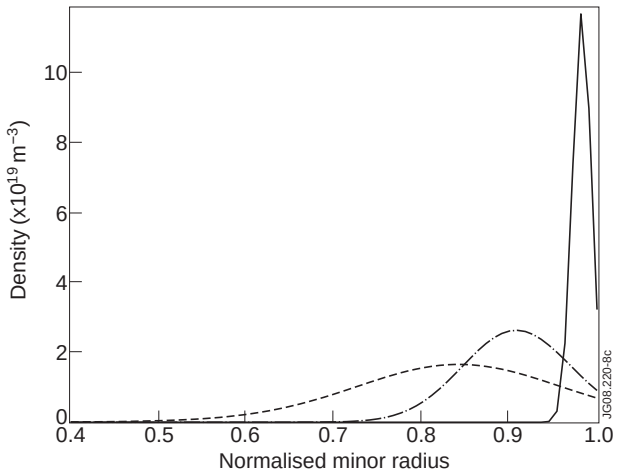

Figure 8: Source profiles for the last injected pellet in 10^{19} m^{-3}; solid- 0% drift, chain - 50% drift, dash - 100% drift.

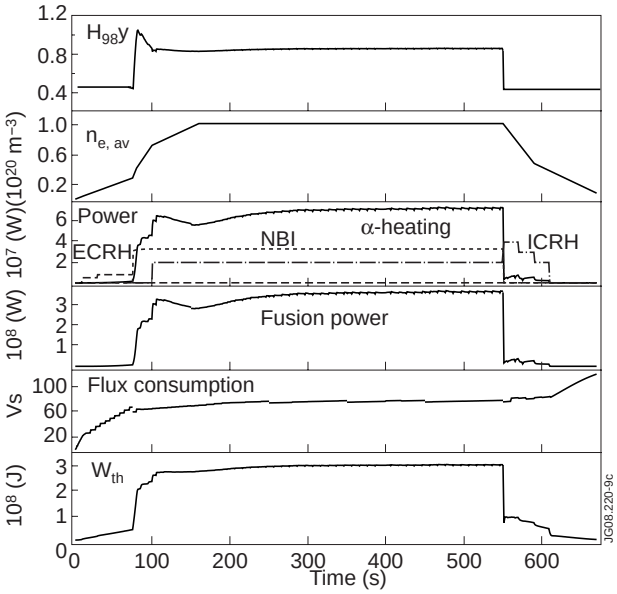

Figure 9: Time traces for predictive modelling of ITER Scenario 2; solid- α-heating power, short dash- NBI power, long dash- ECRH power, chain- ICRH power,

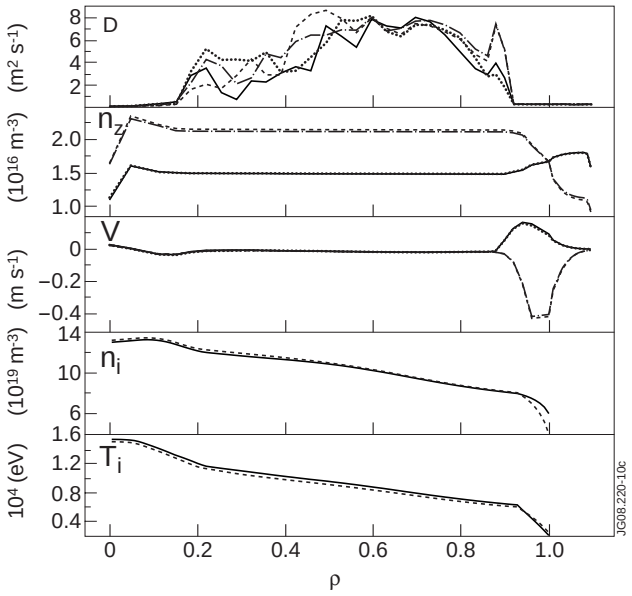

Figure 10:Radial distribution of effective Ar diffusivity: D, (solid- full description, chain line- bundled with 9 super states, solid and dotted - high edge density, dashed and chain - low edge density); total Ar density: n_{Ar}, effective neo-classical pinch velocity for Ar: V_{Ar}, main ion density: n_i and ion temperature: T_i

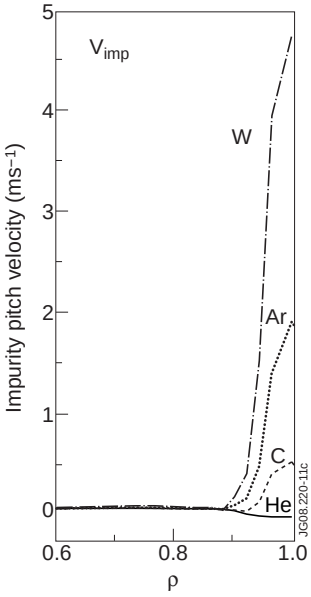

Figure 11:Neo-classical radial pinch velocity for He (solid), C (dashed), Ar (dotted) and W (chain).

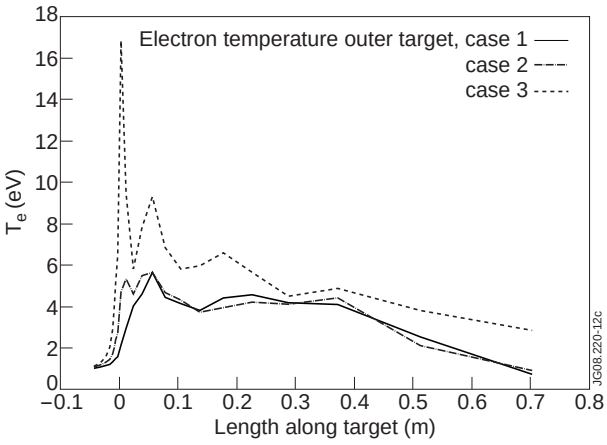

Figure 12: Electron temperature on outer target (solid- "L-mode" , chain- intermediate quality ETB, dash- good quality ETB).

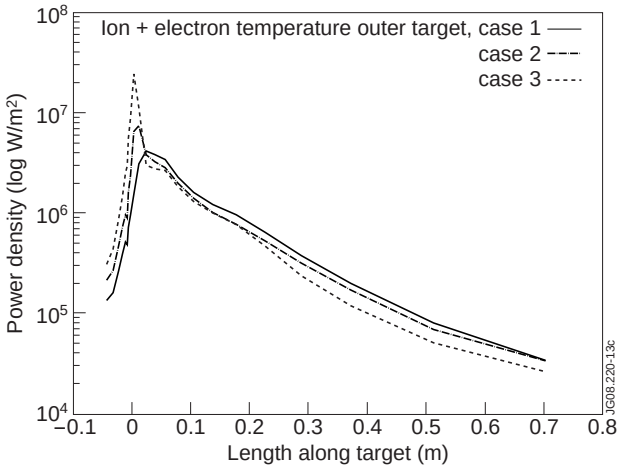

Figure 13: Total power density onto outer target (solid- "L-mode" , chain- intermediate quality ETB, dash- good quality ETB).